

Characterization of Ultra-Wide Bandwidth Wireless Indoor Channels: A Communication-Theoretic View

Moe Z. Win, *Senior Member, IEEE*, and Robert A. Scholtz, *Life Fellow, IEEE*

Invited Tutorial

Abstract—An ultra-wide bandwidth (UWB) signal propagation experiment is performed in a typical modern laboratory/office building. The bandwidth of the signal used in this experiment is in excess of 1 GHz, which results in a differential path delay resolution of less than a nanosecond, without special processing. Based on the experimental results, a characterization of the propagation channel from a communications theoretic view point is described, and its implications for the design of a UWB radio receiver are presented. Robustness of the UWB signal to multipath fading is quantified through histograms and cumulative distributions. The all Rake (ARake) receiver and maximum-energy-capture selective Rake (SRake) receiver are introduced. The ARake receiver serves as the best case (bench mark) for Rake receiver design and lower bounds the performance degradation caused by multipath. Multipath components of measured waveforms are detected using a maximum-likelihood detector. Energy capture as a function of the number of single-path signal correlators used in UWB SRake receiver provides a complexity versus performance tradeoff. Bit-error-probability performance of a UWB SRake receiver, based on measured channels, is given as a function of signal-to-noise ratio and the number of correlators implemented in the receiver.

Index Terms—All Rake receiver (ARake), bit-error probability (BEP), energy capture, propagation channel, selective Rake (SRake) receiver, spread-spectrum, ultra-wide bandwidth (UWB).

I. INTRODUCTION

TECHNIQUES for generating ultra-wide bandwidth (UWB) signals have been known for more than three decades [1]. In the radar community, UWB techniques often are called “carrierless short pulse” techniques. A description of early UWB work can be found in [2]. Recently, there has been a renewed interest in utilizing this technology for UWB

spread-spectrum communications because of its fine delay resolution properties [3]–[16]. These fine delay resolution properties make UWB radio a viable candidate for communications in dense multipath environments [17]–[19]. UWB radios, operating with low transmission power in an extremely large transmission bandwidth, have also been under consideration for future military networks because of their inherent covertness property with low probability of detection and intercept (LPD/LPI) capability [8]–[10].

Propagation environments place fundamental limitations on the performance of wireless communications systems. The existence of multiple propagation paths (multipath) with different delays produces a complex, often time-varying, transmission channel that limits the performance of wireless communications systems. A clear line-of-site path between the transmitter and receiver seldom exists in indoor environments because of natural or man-made blocking and one may have to rely on the signal arriving via multipath or propagating through blockages.

Communication channels have been characterized in terms of dual system functions in the time and frequency domains [20]. There have been texts containing a substantial amount of material on propagation channels [21]–[24] and some texts devoted solely to this subject [25], [26]. Many indoor propagation measurements have been made with much narrower bandwidth signals [27]–[34]. A description of early work on the indoor propagation channels can be found in [34]. Characterization of indoor multipath, including angle of arrival statistics has been described in [35], [36]. Although the work described in this paper does not cover outdoor propagation channels, the selected works on outdoor propagation channels are noted here for their measurement procedures and data reduction techniques [37]–[48].

Narrowband measurements are inadequate for the characterization of UWB signal propagation channels. Specifically, as the bandwidth of the channel probing signal increases, a composite propagation path (at low bandwidth) may be resolved into distinguishable propagation paths (at high bandwidth) with distinct propagation delays. This is equivalent to characterizing the channel transfer function over a broader frequency range.

This paper describes an UWB signal propagation experiment performed in a typical modern office building. A quasi-theoretical/experimental analysis is described and its implications for the design of UWB radio receivers are presented. The UWB propagation analyses in the earlier publications [36], [49] are based on the set of measurements described in this paper.

Manuscript received September 12, 2002; revised October 31, 2002. This work was supported in part by the Joint Services Electronics Program under Contract F49620-94-0022, and in part by the Integrated Media Systems Center, a National Science Foundation Engineering Research Center and the National Science Foundation under Grant 9730556. This paper was presented in part at the IEEE International Symposium on Personal, Indoor, and Mobile Radio Communications, Helsinki, Finland, September 1997, and in part at the IEEE International Conference on Communications, Montréal, Canada, June 1997.

M. Z. Win is with the Laboratory for Information and Decision Systems (LIDS), Massachusetts Institute of Technology, Cambridge, MA 02139 USA (e-mail: moewin@mit.edu).

R. A. Scholtz is with the Communications Sciences Institute, Department of Electrical Engineering-Systems, University of Southern California, Los Angeles, CA 90089-2565 USA (email: scholtz@usc.edu).

Digital Object Identifier 10.1109/JSAC.2002.805031

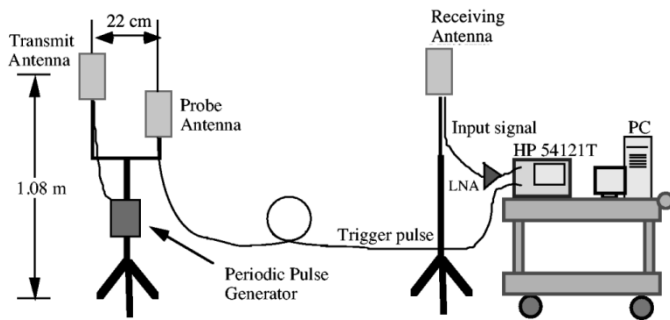


Fig. 1. A block diagram of the measurement apparatus.

II. UWB SIGNAL PROPAGATION EXPERIMENT

A. Experimental Design

In our experiment, a short duration pulse $p(t)$ of approximately one nanosecond duration is transmitted as an excitation signal of the propagation channel. The received signal represents the superposition of distorted replicas of the excitation pulse at different amplitudes and delays. To the extent that they can be identified, each individual path suffers different waveform distortion effects that can occur in UWB signal propagation (e.g., low frequency emphasis in propagation through many materials, and high frequency emphasis in reflections off metallic objects in many instances). Generally, the time varying characteristic of the channel can be observed by periodic retransmission of the probing pulse. The fixed pulse repetition time of this signal must be sufficiently short to characterize the time varying nature of the individually propagating pulses, and long enough to ensure that the multipath response of previous pulse transmissions has decayed before the next transmission.

The duration of a single pulse, inversely proportional to the bandwidth of the transmission, determines the *multipath resolution*, i.e., the minimum differential path delay between individual resolvable multipath components. The period of the periodic pulse signal transmission determines the maximum observable multipath delay. Hence, successive multipath components with differential delay greater than the width of the pulse and within one period of the periodic pulse transmission can be measured unambiguously.

To get maximum benefit from the propagation experiment, we assume that the channel-exciting pulse $p(t)$ is the same waveform that will be used as the fundamental building block of a UWB radio modulation scheme. That is, in a UWB radio used for communication, the transmitted modulation will be a sum of weighted and shifted copies of $p(t)$ [3]–[6]. Under the reasonable assumption that the channel is linear and time-invariant, this implies that the noise-free received signal in the communication receiver can be constructed from the noise-free received propagation measurement over the same channel.

B. Measurement Apparatus

A block diagram of the measurement apparatus is shown in Fig. 1. It consists of a periodic pulse generator that transmits pulses at 500 ns intervals using a step recovery diode-based pulser connected to a UWB antenna. A 500-ns pulse repetition time was sufficient to capture all the significant multipaths

as will be shown in the next section. A transmitting antenna is connected to the pulse generator via a coaxial cable, with ferrite beads mounted at each end of the coaxial cable for isolation. The receiver consists of a vertically polarized receiving antenna, wideband low noise amplifier (LNA), attenuator, and digital sampling oscilloscope (DSO). The attenuator provides a safety margin for the DSO and prevents the DSO from being damaged. Multipath profiles are captured by the DSO and sent over an interface bus to a personal computer for storage.

The triggering signal from the probe antenna, in close proximity to the transmit antenna, is supplied to the receiver apparatus by a long *fixed-length* coaxial cable. The length of this coaxial cable is 200 feet and the propagation delay in the coaxial cable is measured to be 250.6 ns.¹ Therefore, all recorded multipath profiles have the same absolute delay reference, and precise propagation delay measurements of the signals arriving at different receiving antenna locations can be made.

Initial measurements indicated that some multipath response profiles contain significant energy beyond 250 ns depending on the specific location of the transmitter and the receiver. This means that the measurement window must be at least 250 ns wide. However a DSO is only capable of capturing a certain number of samples in each measurement scan. Because of the limited buffer size of the DSO, multipath data collected over a large observation window would result in a large gap between samples. Therefore, 50-ns long windows of multipath data are collected and later concatenated by a computer program to get a data record of the desired size with good resolution (fine detail in the delay domain). The DSO is set in such a way that every 50-ns window of measurements contains 1024 samples throughout the experiments. This implies that the time between samples is 48.828 ps and the equivalent sampling rate is 20.48 GHz. Therefore, according to the sampling theorem, any signals with bandwidth below 10 GHz can be reproduced from the samples collected by the DSO [50]–[56].

The DSO has the internal capability to average over several received waveforms for noise reduction purposes. Taking advantage of this capability, 32 sequentially measured multipath profiles are averaged and recorded along with raw (unaveraged) multipath profiles at every measurement location. During each of the multipath profile measurements, both the transmitter and receiver are kept stationary. The multipath propagation channel is “frozen” during the measurement time by making sure that people in the vicinity of the transmitter and receiving antenna have stopped moving. Indeed over 50% of the measurements are collected during the evenings and weekends when most people are not present. To insure the quality of recorded data, every multipath profile is inspected in detail using the zoom capability of data acquisition software before storing for further data reduction.

C. Measurement Results

Propagation measurements were made on one floor of a modern laboratory/office building having the floor plan shown in Fig. 2. Each of the rooms is labeled alphanumerically. Walls

¹Because the delay in the coaxial cable is longer than the free-space propagation time from transmitter to receiver, the pulse supplied by the cable serves as a trigger for the propagation measurement of the next transmitted pulse.

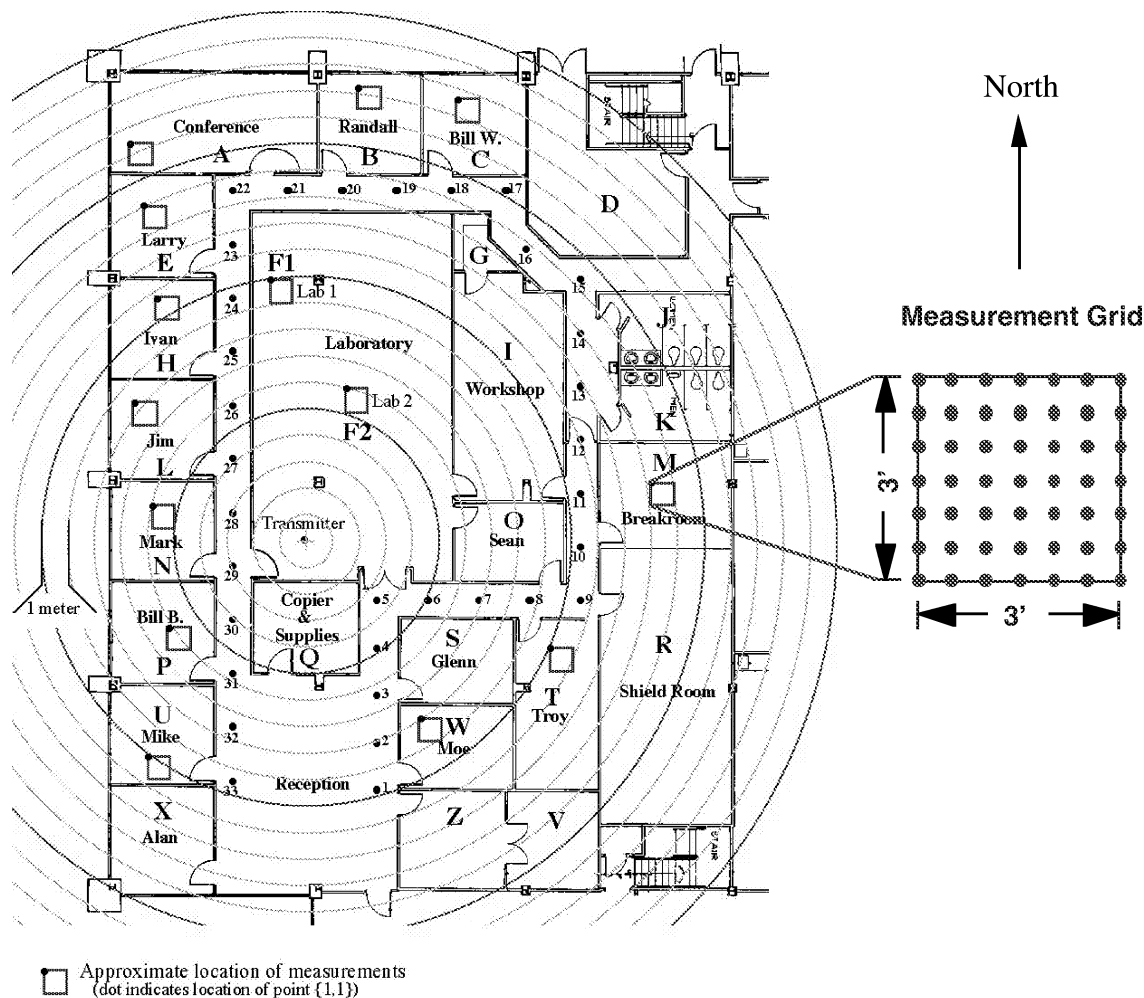


Fig. 2. A diagram of the modern office building where the propagation measurement experiment was performed. The concentric circles are centered on the transmit antenna and are spaced at 1-m intervals.

around offices are framed with metal studs and covered with plaster board. The wall around the laboratory is made from acoustically silenced heavy cement block. There are steel core support pillars throughout the building, notably along the outside wall and two in the laboratory itself. The shield room's walls and door are metallic. The transmitter is kept stationary in the central location of the building in a laboratory denoted by F. The transmit antenna is located 165 cm from the floor and 105 cm from the ceiling.

Fig. 3 shows the transmitted pulses measured by the receiving antenna, located 1 m from the transmitting antenna at the same height. The antennas used in this experiment were diamond dipoles [57]. Measurements were made while the vertically polarized receiving antenna was rotated about its axis in 45° steps. Measurements shown in Fig. 3 are labeled 0° , 45° , and 90° , where 0° refers to the case in which the planes of the transmitting and receiving antennas are parallel. The packaged antennas, which are flat and roughly the size of a playing card, display nearly circularly symmetric dipole-like radiation patterns about their vertical axes. The building floor plan of Fig. 2 indicates that the closest object to the measurement apparatus is the south wall of laboratory F, which is at least 1 m away. The signal arriving at the receiving antenna, except for the line-of-sight

(LOS) signal, must travel a minimum distance of 3 m. The initial multipaths come from the floor and ceiling, 5.2 and 4.1 ns after the LOS signal, respectively, and hence the first 10 ns of the recorded waveforms in Fig. 3 represent clean pulses arriving via the direct LOS path and not corrupted by multipath components.

Multipath profiles are measured at various locations in the rooms and hallways throughout one floor of the building. Specifically, data was collected in 14 different rooms and along the hallways. In each room, 300 ns-long response measurements are made at 49 different locations in one square yard. The approximate location of these measurement grids in each room is shown in Fig. 2. They are arranged spatially in a level 7×7 square grid with 6 inch spacing between measurement points. Each location on the grid is numbered as (i, j) , where i represents the row index and j represents the column index of the grid. As a convention, the first row is always parallel and adjacent to the north wall of the room. The receiving antenna is located 120 cm from the floor and 150 cm from the ceiling. This antenna height is envisioned to be typical for future indoor applications. A single multipath profile of 1000 ns duration, which captures the response of two successive probing pulses, is also made in each room. This is

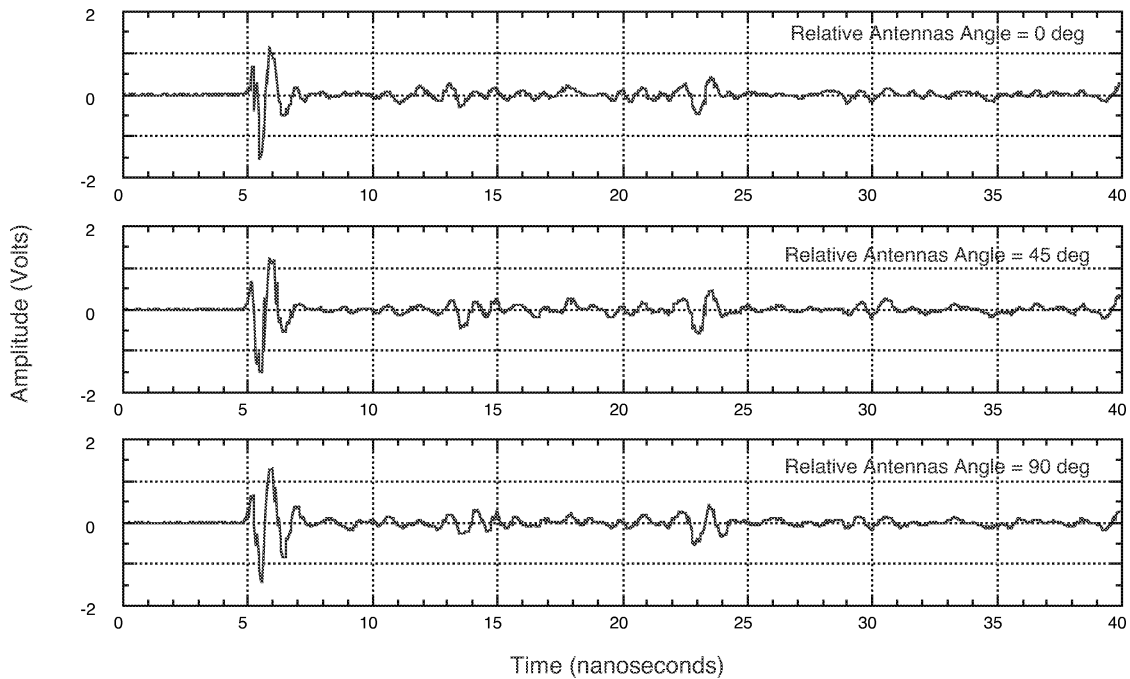


Fig. 3. Transmitted pulses measured by the receiving antenna located 1 m away from transmit antenna with the same height. The receiving antenna is rotated around its vertical axis to make measurements where 0° refers to the case in which the planes of the transmit and the receiving antennas are parallel.

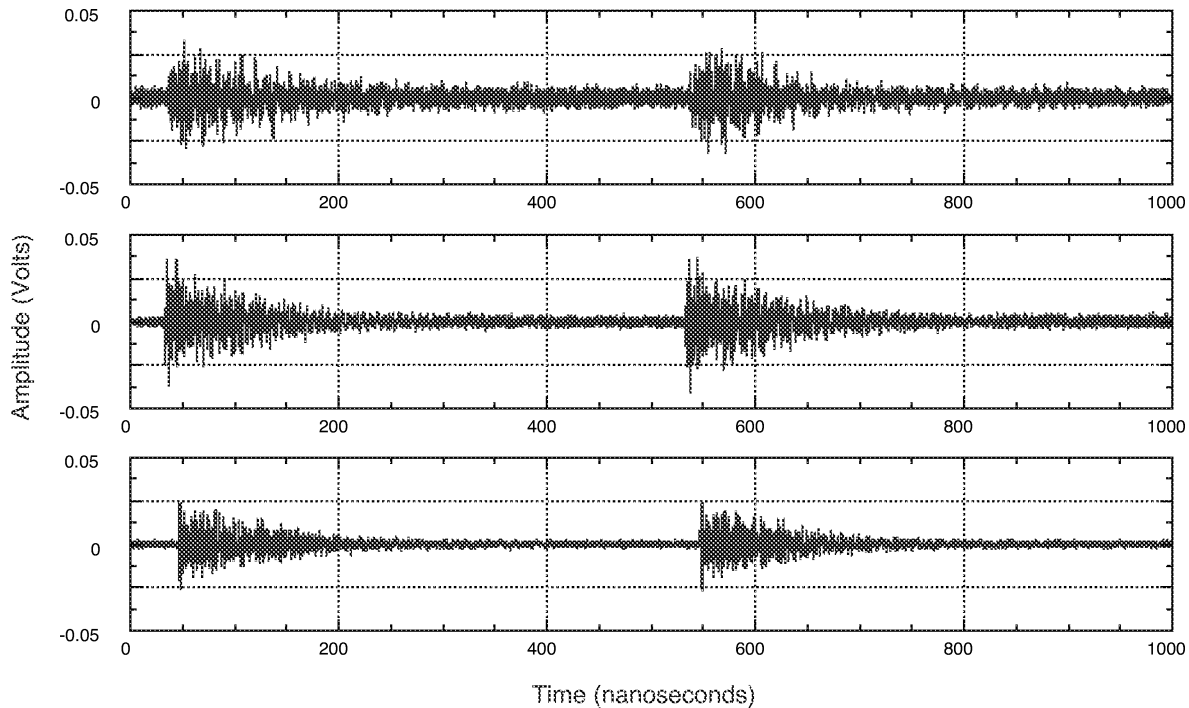


Fig. 4. Two back-to-back-cycles of 1000 ns-long averaged multipath measurement captured by the receiver located in offices U (upper trace), W (middle trace), and M (lower trace) where the measurement grids are 10, 8.5, and 13.5 m away from the transmitter, respectively.

to verify that multipath profiles of the first probing pulse have decayed before the response to the next pulse arrives at the receiving antenna.

Fig. 4 shows the 1000 ns-long measurement, where two back-to-back multipath measurement cycles are captured by the receiver located in offices U, W, and M, respectively. The approximate distances between the transmitter and the location

of these measurement grids located in offices U, W, and M are 10, 8.5, and 13.5 m, respectively. Fig. 4 also shows that the response of the first probing pulse has decayed before the next pulse arrives at the antenna. An excess delay on the order of 100 ns occurs in these situations.

Substantial differences in the measurement noise level at various locations throughout the building can also be observed from

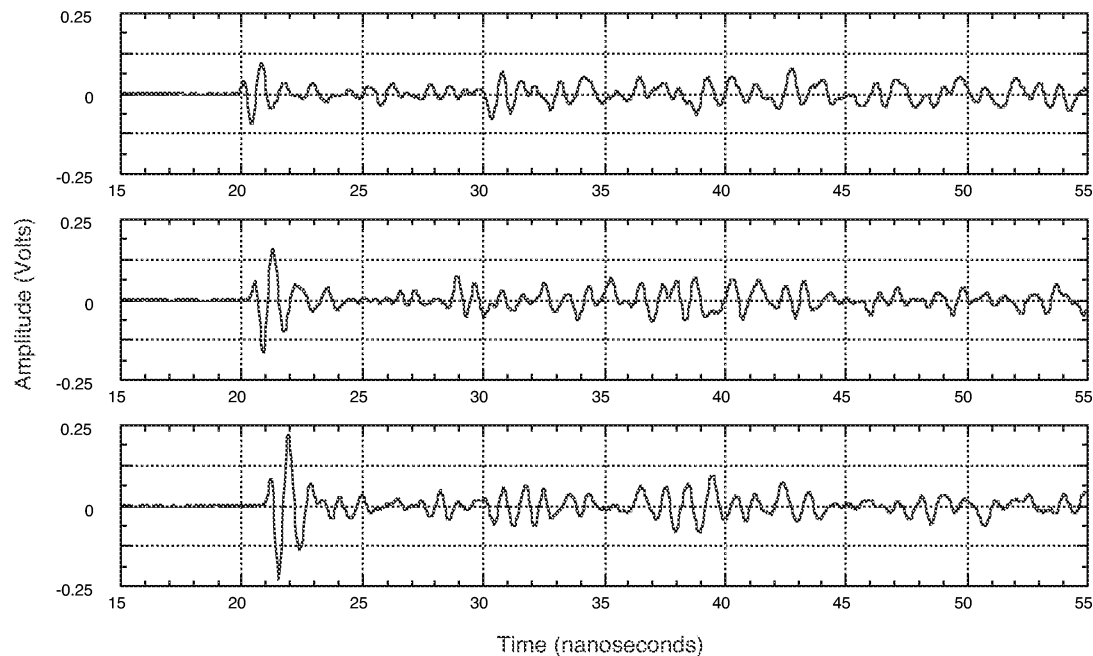


Fig. 5. Averaged multipath profiles over a 40 ns window measured at (4,1), (4,4), and (4,7) of the grid denoted by F2 in building floor plan of Fig. 2. The first arriving signal of the top trace is shadowed by the steel core support pillar located between the transmitter and the receiver.

Fig. 4. Specifically, the multipath profiles recorded in the offices W and M have a substantially lower noise level compared with the profiles recorded in office U. This can be explained, with the help of the building floor plan given in Fig. 2, by observing the following. Office U is situated at the edge of the building with a large glass window and is subject to more external interference. Offices W and M are situated roughly in the middle of the building. Furthermore, office W is situated in the vicinity of room R and office M is adjacent to room R which is shielded from electromagnetic radiation. Therefore, most of the interference from radio stations, television stations, cellular and paging towers and other external electromagnetic interference (EMI) sources is attenuated by the shielded walls and multiple layers of other regular walls. In general, an increased noise floor is observed for all the measurements made in offices located at edges of the building with large glass windows.

Fig. 5 shows the measurements at (4,1), (4,4), and (4,7), i.e., three different positions one foot apart along a horizontal line of the grid, denoted by F2 in Fig. 2. Note that the receiver and transmitter are located in the same room. It can be seen in Fig. 5 that the first arriving peak of the signal level increases as the receiving antenna moves from (4,1) to (4,7). This can be attributed to the shadowing by the steel core support pillar located between the transmitter and the receiver as seen in the building floor plan of Fig. 2.

Fig. 6 shows the 40 ns long averaged multipath profiles measured at the center of the measurement grid at position (4,4) in offices P, H, and B. The approximate distances between the transmitter and the receiving antenna positions in offices P, H, and B are 6, 10, and 17 m, respectively, representing typical UWB signal transmission paths for the “high signal-to-noise ratio (SNR),” “low SNR,” and “extreme low SNR” environments as we have named them. Notice that the first arriving multipath component is *not* always the strongest multipath

component. A total of 741 different multipath profile measurements are made at various locations (12 different rooms with 49 locations/room, 2×49 locations in the lab, 21 locations in the shield room, and 34 locations around the hallways).

D. Miscellaneous Results

To understand the effect of office doors, two multipath profiles were recorded at the same location in office B. One profile was recorded with the office door open and the other with the office door closed, however no noticeable difference between these two situations was observed in this experiment.

The effect of microwave oven leakage is observable. There were two microwave ovens located in break room M and one located in supply room Q. Some multipath propagation measurements were made while either of the microwave ovens was operating. It was observed that microwave ovens significantly corrupt the multipath profile measurements even when the receiver is located several meters (and a few walls) away from the operating microwave oven.

The effect of a large computer monitor was also considered. When the receiving antenna was placed near a large computer monitor in office C, a slight increase in noise floor was observed when the computer monitor was turned on.

III. CHARACTERIZATION OF THE UWB PROPAGATION CHANNEL

A statistical characterization of the propagation channel often is useful in communication systems engineering, e.g., in deriving optimal reception methods, estimating the system performance, performing design tradeoffs, etc. In this section, characterization of the UWB propagation channel is done, based on 741 measured multipath profiles described in Section II-C.

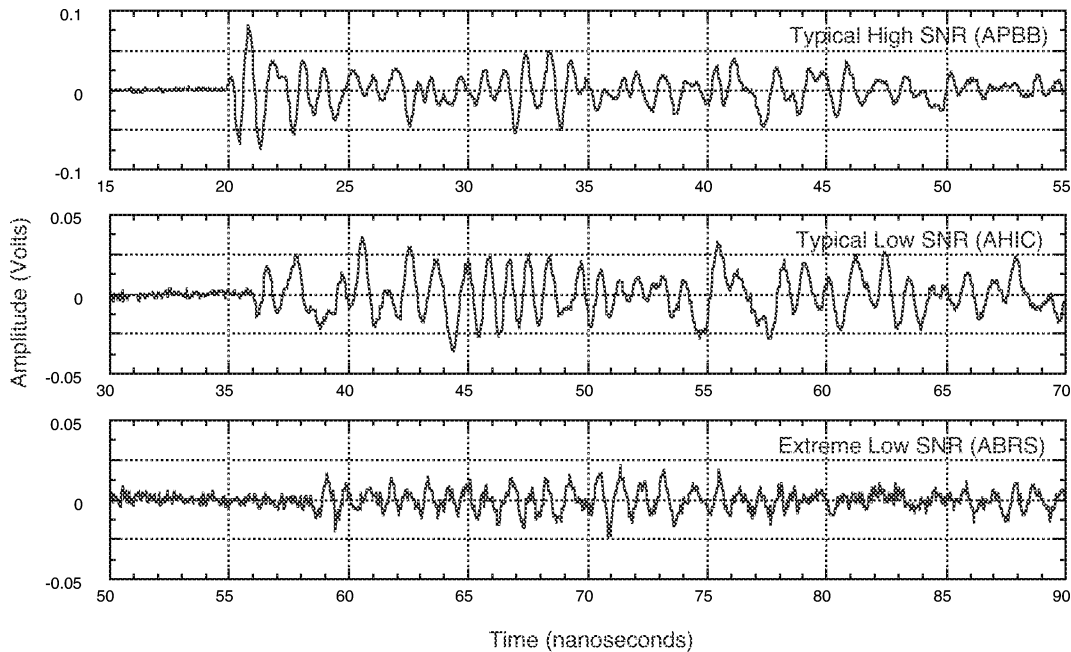


Fig. 6. Averaged multipath profiles over a 40 ns window measured at the center of the measurement grid in offices P (upper trace), H (middle trace), and B (lower trace). The positions of the receiving antenna in offices P, H, and B are located 6, 10, and 17 m away from the transmitter, respectively, representing typical UWB signal transmission for the “high SNR,” “low SNR,” and “extreme low SNR” environments.

Each measured multipath profile or received signal $r(u, t)$ can be written as

$$r(u, t) = s(u_s, t) + n(u_n, t) \quad (1)$$

where $n(u_n, t)$ represents the receiver noise as well as the undesired interference. The quantity $s(u_s, t)$ is the channel response to the transmitted UWB signal in the absence of undesired interference and receiver noise.² For the case of free-space propagation (absence of multipath) $s(u_s, t) = c(u_s)w(t)$, where $w(t)$ is the ideal received waveform, and $c(u_s)$ models the free-space path loss. The parameter u indexes the outcome of the stochastic environment $\Omega = \Omega_s \times \Omega_n$, where $u = (u_s, u_n)$ with $u_s \in \Omega_s$ and $u_n \in \Omega_n$.³ The stochastic environment Ω in the context of this paper is a measurement experiment performed in an office building, where $r(u, t)|_{u=\tilde{u}=(\tilde{u}_s, \tilde{u}_n)}$ denotes a *particular* observation, $s(u_s, t)|_{u_s=\tilde{u}_s}$ denotes the channel response to the transmitted UWB pulse at a *specific* position \tilde{u}_s inside an office, and $n(u_n, t)|_{u_n=\tilde{u}_n}$ is the *observation* noise. Since the measurement process of $r(u, t)$ is carried out using a DSO, the measurement noise $n(u_n, t)$ can be modeled as additive white Gaussian noise (AWGN).

The UWB radio design problem is closely coupled to details of the channel characterization. For example, in a known channel with AWGN and no intersymbol interference, an optimal UWB radio should perform coherent detection of the possible received data signals. Therefore, the optimum synchronous receiver is a matched filter or correlation receiver [60] in which correlator reference signals are constructed from copies of the

²The UWB signals $s(u_s, t)$ in this experiment occupy a wide bandwidth centered around 1 GHz. The recent ruling [58] by the United States Federal Communications Commission restricts UWB communication activity to the frequency band between 3.1 and 10.6 GHz. This difference in band occupancy should be considered in using the results contained herein.

³The product space Ω can be defined rigorously [59].

noise-free pulse-response function $s(\tilde{u}_s, t)$ of the channel in the same way that the transmitted modulation is constructed from copies of the transmitted pulse $p(t)$.

For a specific observation $r(u, t)|_{u=\tilde{u}}$ in the presence of multipath, the question of channel characterization from a Rake receiver design viewpoint is how well one can match the signal $s(u_s, t)|_{u_s=\tilde{u}_s}$ with a template consisting of a linear combination of delayed versions of a synthesizable waveform $w(t)$. Note that fundamental building block $w(t)$ of a UWB receiver ideally should resemble the shape of waveforms received over a single propagation path.⁴ Specifically, the template waveform built into the receiver for use in Rake correlator structures is modeled as [63], [64]

$$\hat{s}(u, t) = \sum_{i=1}^L \hat{c}_i(u)w(t - \hat{\tau}_i(u)). \quad (2)$$

The parameters $\hat{c}_i(u)$ and $\hat{\tau}_i(u)$ are modeled as random variables with $\hat{c}_i(u) \in \mathbb{R}$ and $\hat{\tau}_i(u) \in \mathbb{R}^+$.⁵

Characterizations of the propagation channel can be separated into two categories, namely (A) non model-based characterizations and (B) model-based characterizations. Both of these approaches will be considered in the following sections.

A. Non Model-Based Multipath Channel Characterization

As the name implies, non model-based channel characterization is carried out *without using a specific model* for the multipath channel. There are no models used or assumptions made about the structure of the signal $s(u_s, t)$ (such as (2) that resulted from specular multipath propagation).

⁴Even under ideal free-space propagation conditions, the received waveform may not look like the waveform driving the transmitting antenna. For examples of such transmission effects, see [61], [62].

⁵The usual notation for $\mathbb{R} = (-\infty, +\infty)$ and $\mathbb{R}^+ = [0, +\infty)$ is used.

TABLE I
SIGNAL QUALITY STATISTICS

Room	\approx distance (meters)	Minimum (dB)	Maximum (dB)	$\hat{\mu}$ (dB)	Median (dB)	$\hat{\sigma}$ (dB)	# of Samples
F2	5.5	-12.9970	-9.64586	-11.5241	-11.6813	0.8161	49
N	5.5	-16.0060	-13.2949	-14.7260	-14.7690	0.5892	49
P	6.0	-15.5253	-12.2185	-14.2373	-14.2820	0.8091	49
L	8.0	-16.6966	-12.4310	-14.4500	-14.5538	0.8342	49
W	8.5	-20.0157	-17.0351	-18.7358	-18.7425	0.7622	49
F1	9.5	-14.4064	-9.79770	-12.0986	-12.1407	1.0563	49
H	10.0	-21.0415	-16.1628	-18.7141	-18.8142	1.1240	49
U	10.0	-21.1719	-17.6232	-19.4275	-19.4092	0.8024	49
T	10.5	-21.9113	-19.2986	-20.6100	-20.5419	0.5960	49
R	10.5	-23.7221	-20.8867	-22.2675	-22.3851	0.8686	21
M	13.5	-23.8258	-20.9277	-22.2568	-22.2064	0.6439	49
E	13.5	-24.1454	-20.2000	-22.5973	-22.7824	1.0332	49
A	16.0	-25.4171	-20.7822	-23.2826	-23.3541	1.1512	49
B	17.0	-24.7191	-21.2006	-22.9837	-22.9987	0.8860	49
C	17.5	-26.4448	-22.3120	-24.4842	-24.5777	1.0028	49
Hallways		-23.8342	-6.72469	-16.9317	-17.3286	4.5289	34

1) *Robustness of the UWB Signal in Multipath:* Robustness of the UWB signal to multipath can be assessed by measuring the received energy in various locations of the building relative to the received energy at a reference point. Mathematically, the *signal quality* can be defined as

$$Q(u) = 10 \log_{10} E_{\text{tot}}(u) - 10 \log_{10} E_{\text{ref}} \quad [\text{dB}]. \quad (3)$$

The received energy $E_{\text{tot}}(u)|_{u=\tilde{u}}$ at a specific measurement position \tilde{u} is given by

$$E_{\text{tot}}(\tilde{u}) = \int_0^T |r(\tilde{u}, t)|^2 dt \quad (4)$$

where $r(\tilde{u}, t)$ is the measured multipath profile at the position \tilde{u} (e.g., at a particular location (i, j) in the measurement grid) and T is the observation time (300 ns). The reference energy E_{ref} is chosen to be the energy in the LOS path measured by the receiver located 1 meter away from the transmitter.

The variable $Q(u)$ is calculated for the measurements made at 741 different locations in the building of Fig. 2. First and second-order local statistics of the signal quality are calculated. That is, the mean and variance of the signal quality based on measurements at collections of spatial sample points in each room are estimated by

$$\hat{\mu} = \frac{1}{N} \sum_{u \in \mathcal{U}_{\text{room}}} Q(u) \quad (5)$$

and

$$\hat{\sigma}^2 = \frac{1}{N-1} \sum_{u \in \mathcal{U}_{\text{room}}} (Q(u) - \hat{\mu})^2 \quad (6)$$

where $\mathcal{U}_{\text{room}}$ is the set of measurements within a room and $N = |\mathcal{U}_{\text{room}}|$.⁶

Table I shows the estimates $\hat{\mu}$, $\hat{\sigma}$ of the mean and standard deviation of the signal quality in each room, based on the samples taken in that area. The histogram and cumulative distribution function (CDF) of the signal quality for measurements made in these locations are shown in Fig. 7. This data indicates that the signal energy per received multipath waveform varies by at most 5 dB as the receiving position varies over the measurement grid within a room. This is considerably less than the fading margin employed in most narrowband systems, and indicates the potential of UWB radios for robust indoor operation at low transmitted power levels.

2) *All Rake Receiver:* The ultimate goal of a Rake receiver is to construct correlators or filters that are matched to the set of received symbol waveforms corresponding to a train of transmitted pulses. If the propagation measurement process is carried out by sounding the channel with the same pulses and the same antennas from which an UWB communication system constructs its transmission signal, then, the measurements can be used directly to estimate the performance and to determine the various design aspects of an UWB communication system.

Imperfect construction of the synthesized waveform $s(u_s, t)$ in a UWB Rake receiver can degrade the performance of the receiver. These imperfections can be attributed in part to practical hardware constraints which limit the finite number of correlators

⁶If the received signal energies $E_{\text{tot}}(u)$ are random samples from normal families, it can be shown that these estimates are functions of complete sufficient statistics. Then by the Lehmann-Scheffé theorem [65], the estimates given by (5) and (6) are unique uniformly minimum-variance unbiased estimates.

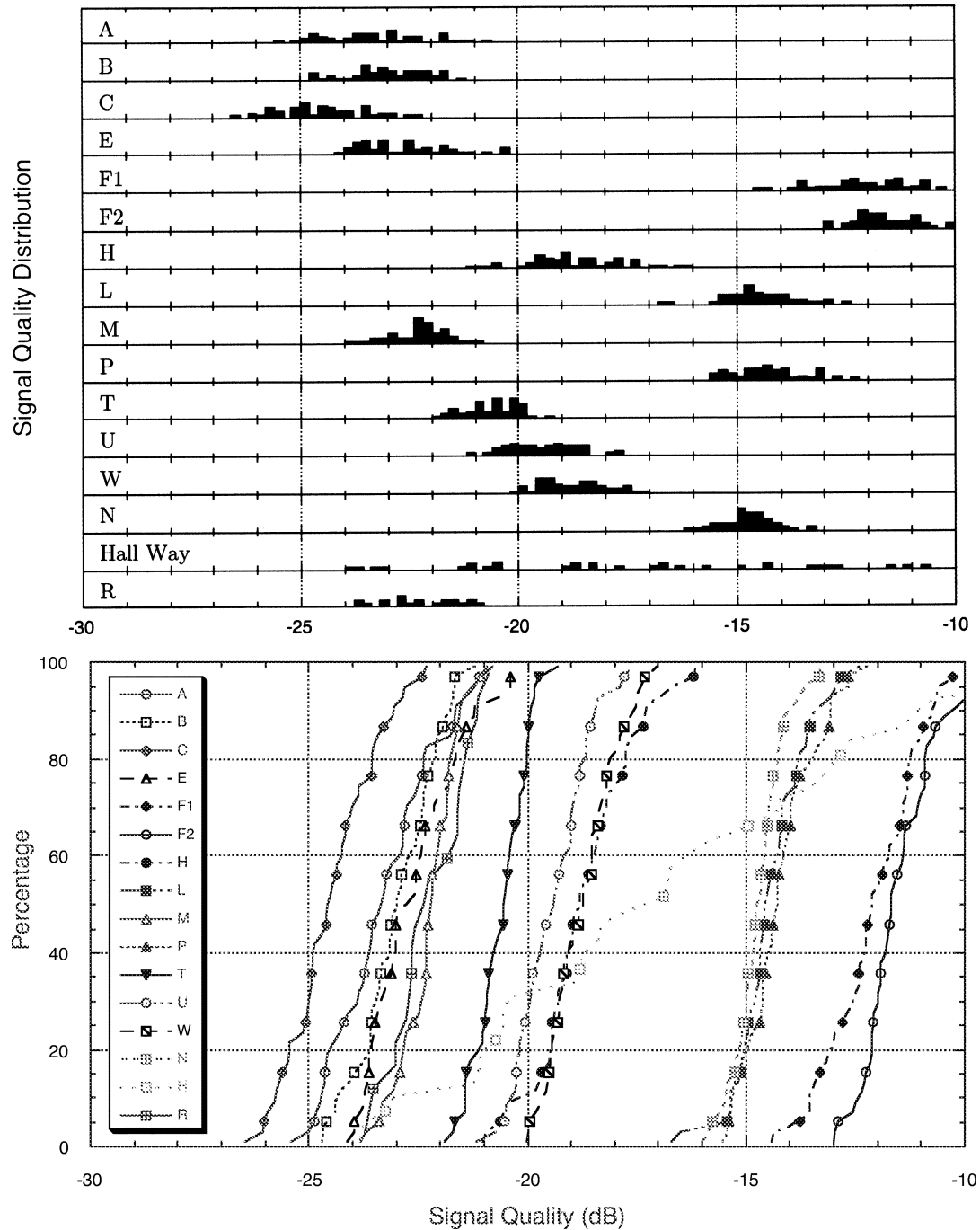


Fig. 7. The histogram (upper plot) and cumulative distribution function (lower plot) of the signal quality based on 49 spatial sample points (except 21 spatial points for room R and 34 spatial points for hallways) in each room. A total of 741 measurements are used in these plots.

available in a Rake receiver architecture.⁷ The degradation due to the multipath channel can be separated from the effect of imperfect construction of the synthesized waveform by considering the *all Rake* (ARake) receiver. The ARake receiver is a Rake receiver with unlimited resources (correlators) and instant adaptability, so that it can, in principle, perfectly construct matched filters or correlator reference signals that are identical to the set of received symbol waveforms. Although this

⁷This issue is closely related to the design of “selective Rake” receiver architectures [66]–[72] and is addressed in the next section.

is not practical, an ARake receiver serves as the best case (benchmark) for Rake receiver design.

The performance of any ideal synchronous receiver operating over a single-link AWGN channel depends on the autocorrelation matrix of the signal set. When the multipath spread is much less than the pulse spacing during transmission, the effect of intersymbol and interpulse interference is negligible and, hence, this autocorrelation matrix and an appropriately defined SNR are the only quantities determining the performance of an optimal receiver. Hence, the performance of such a perfectly synchronized UWB ARake receiver in a multipath environment

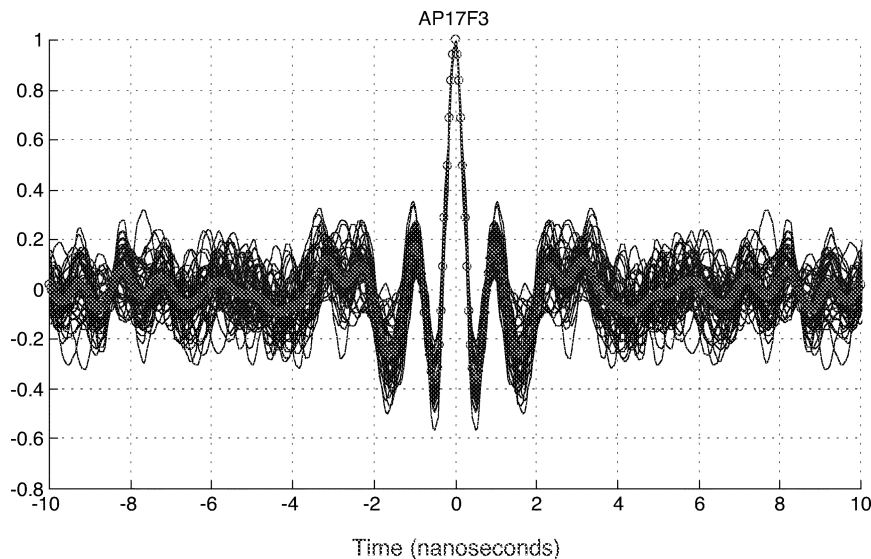


Fig. 8. Joint normalized plot of 49 different $R_{\text{ARake}}(\zeta)$ functions obtained in room P. The transmitter is approximately 6 m from the receiver representing typical UWB signal transmission for the “high SNR” environment.

can be predicted by computing the autocorrelation function $R_{\text{ARake}}(\zeta)$ of a noise-free channel response $s(u_s, t)$

$$R_{\text{ARake}}(\zeta) = \int_0^T s(u_s, t) s(u_s, t - \zeta) dt \quad (7)$$

and appropriately sampling this function to construct the autocorrelation matrix of the signal set used by the UWB radio [73]. In an ideal channel (in the absence of multipath), the correlation function is given by

$$R_{\text{Ideal}}(\zeta) = c^2(u_s) \int_0^T w(t) w(t - \zeta) dt \quad (8)$$

where $w(t)$ is the sounding signal seen at the receiving antenna output in the absence of multipath. As pointed in Section II-C, measurements made in the offices located in the interior part of the building have a lower noise floor. Furthermore, averaging the multipath profiles that are sequentially collected at a fixed location effectively suppresses the observation noise. In this case $s(u_s, t) \approx r(u, t)$. Then, R_{ARake} becomes

$$R_{\text{ARake}}(\zeta) \approx \int_0^T r(u, t) r(u, t - \zeta) dt. \quad (9)$$

The function $R_{\text{ARake}}(\zeta)$ is computed for each of the 741 different measurement locations using the approximation (9). Its local variation can be assessed by jointly displaying the normalized plot of different $R_{\text{ARake}}(\zeta)$ functions for the 49 measurement points in each room. Fig. 8 shows the normalized plots of different $R_{\text{ARake}}(\zeta)$ functions in room P. This illustrates a typical ensemble of autocorrelation functions that must be considered in choosing a data modulation technique. As one would expect, when normalized to equal energy these correlation functions look approximately the same for values of the shift parameter ζ less than a transmitted pulse width (< 1 ns). However, these correlation functions vary considerably for larger values of ζ because the set of differential path delays varies for dif-

ferent points on the measurement grid. This implies that the autocorrelation matrix of the signal set used by the UWB radio is a random matrix with entries consisting of various samples of the correlation function.

For values of ζ larger than the transmitted pulse width, these plots of $R_{\text{ARake}}(\zeta)$ may look quite different for different rooms. For the pulse used to sound rooms and produce the curves of Fig. 8, a reasonable amount of time shift for 2-level pulse position modulation (PPM) is the location of the first aggregate minimum next to the peak in these curves, i.e., roughly 0.5 ns. Notice that the performance prediction [for example, bit-error probability (BEP)] will vary somewhat from position to position within the measurement grid since the autocorrelation matrix of the signal set is a random matrix with varying entries from position to position. This technique of using measured multipath profiles to evaluate signal designs has been used to compare the BEP performance of different possible 4-ary PPM designs [74].

B. Model-Based Multipath Channel Characterization

Channel characterization for Rake receiver design can be carried out using a *finite specular-multipath channel model* $\hat{s}(u_s, t)$ given in (2) for the signal $s(u_s, t)$. This model is used by the receiver in its construction of the Rake signal processor with fundamental building block waveform $w(t)$. The actual environment that creates the multipath signal may not realistically be viewed as containing only L_b reflectors and, hence, the model cannot perfectly represent $s(u_s, t)$.

In general, the number of resolvable path components in a realistic dense multipath channel (especially in an indoor channel) is roughly proportional to the transmission bandwidth W and the excess delay T_d of the channel. While the product WT_d may be large for a UWB signal transmission, only a small fraction of these resolvable multipath components may be necessary in the receiver’s signal model to ensure the utilization of a reasonable fraction of the energy available in a received symbol waveform.

1) *A Specular Multipath Channel Model:* An efficient Rake receiver using a specified number of correlators, L , is based on

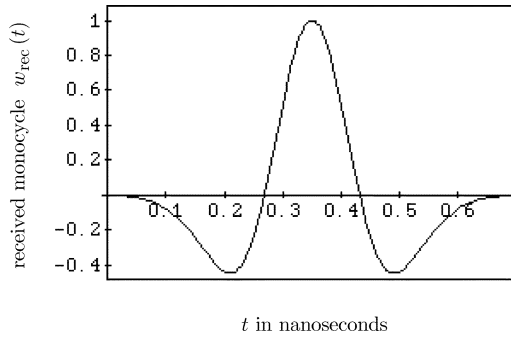


Fig. 9. A typical idealized received waveform as a function of time in nanoseconds. The model used in this plot is $w(t + .35) = [1 - 4\pi(t/\tau_m)^2] \exp[-2\pi(t/\tau_m)^2]$ with $\tau_m = 0.2877$, which is assumed to be reasonably well matched to the isolated paths in the whole ensemble of measured received waveforms.

a specular L -path model for the channel that best matches the waveform $s(u_s, t)$. The number L is proportional to the complexity of receiver's demodulator. In the existing literature, this is typically accomplished by discretizing the delay axis into bins of width $\Delta\tau$ seconds. If the integrated power c_i^2 , within the interval of i^{th} delay bin, of the received signal $r(u, t)$ exceeds the chosen minimum detectable signal threshold, a multipath component with magnitude $|c_i|$ is said to exist at delay $i\Delta\tau$. The L paths corresponding to the largest values of $|c_i|$ may then be chosen as the dominant paths [28].

The number of multipath components also influences the choice of channel modeling techniques. If the number of multipath components is small (≈ 5), then, they can be attributed to obvious reflecting objects in the radio system environment, and a ray tracing model based on the building geometry is a plausible choice. On the other hand, ray tracing techniques becomes site specific and their computational complexity becomes a burden when the number of multipath components is large [28].

In this paper, a modeling approach motivated by Rake receiver design is used, i.e., it is desired to model the received multipath profile $s(u, t)$ by $\hat{s}(u, t)$ [see (2)], a finite linear combination of delayed versions of a basic waveform $w(t)$. A shape often used as a model of the waveform $w(t)$ is shown in Fig. 9, although this waveform can vary considerably, depending on the antenna design, the excitation used in the transmitter, and the relative optimality of the receiver processing. Here, it is assumed that the shape of $w(t)$ is reasonably similar to the isolated path signals in the whole ensemble of measured received waveforms.

The ARake receiver is not realizable. In fact, as the resolution of a radio system becomes finer, performance approaching that of an ARake receiver becomes more difficult to achieve because of the increased number of paths required in a specular model. Complexity and performance issues have motivated studies of *selective Rake* (SRake) receivers that process only a *subset* of the available resolved multipath components [66]–[72]. These receivers diversity combine the outputs of a fixed number of correlators, each selectively locked to a different resolved signal path. Of course the delay and amplitude parameters of each selected path in the model must be estimated by the receiver's Rake processor.

2) *The Optimal Multipath Detector*: Given a specific received signal $r(\tilde{u}, t)$ over an observation interval $[0, T)$ and a fixed value of L , the objective of a SRake processor is to find the “best” values of $\{\hat{c}_i(\tilde{u})\}_{i=1}^L$ and $\{\hat{\tau}_i(\tilde{u})\}_{i=1}^L$, such that the synthesized template $\hat{s}(\tilde{u}, t) = \sum_{i=1}^L \hat{c}_i(\tilde{u})w(t - \hat{\tau}_i(\tilde{u}))$ is well matched to the received waveform $r(\tilde{u}, t)$.

In this paper, the maximum-likelihood (ML) technique is considered as the optimality criterion. For a given L , let \mathbf{c} and $\boldsymbol{\tau}$ be the amplitude and the delay vectors, with dimension $L \times 1$, defined by

$$\mathbf{c} \triangleq \begin{bmatrix} c_1 \\ c_2 \\ \vdots \\ c_L \end{bmatrix} \quad \text{and} \quad \boldsymbol{\tau} \triangleq \begin{bmatrix} \tau_1 \\ \tau_2 \\ \vdots \\ \tau_L \end{bmatrix}. \quad (10)$$

Since $n(u_m, t)$ is modeled as AWGN, the ML criterion is equivalent to a minimum-mean-squared error (MMSE) criterion. Thus, the ML estimates of the amplitude vector $\hat{\mathbf{c}}(\tilde{u})$ and delay vector $\hat{\boldsymbol{\tau}}(\tilde{u})$ based on a specific observation $r(\tilde{u}, t)$ are the values $\mathbf{c}(\tilde{u})$ and $\boldsymbol{\tau}(\tilde{u})$ which minimize the following mean-squared error

$$\mathcal{E}(\tilde{u}, L) = \int_0^T \left| r(\tilde{u}, t) - \sum_{i=1}^L c_i w(t - \tau_i) \right|^2 dt. \quad (11)$$

The minimum value of the above mean-squared error is denoted by $\mathcal{E}_{\min}(\tilde{u}, L)$.

The ML estimates of the delay vector $\hat{\boldsymbol{\tau}}$ and amplitude vector $\hat{\mathbf{c}}$ are derived in Appendix A as

$$\hat{\boldsymbol{\tau}}(\tilde{u}) = \underset{\boldsymbol{\tau}}{\operatorname{argmax}} \left\{ \boldsymbol{\chi}^\dagger(\tilde{u}, \boldsymbol{\tau}) \mathbf{R}^{-1}(\boldsymbol{\tau}) \boldsymbol{\chi}(\tilde{u}, \boldsymbol{\tau}) \right\} \quad (12)$$

and

$$\hat{\mathbf{c}}(\tilde{u}) = \mathbf{R}^{-1}(\hat{\boldsymbol{\tau}}(\tilde{u})) \boldsymbol{\chi}(\tilde{u}, \hat{\boldsymbol{\tau}}(\tilde{u})) \quad (13)$$

where $\mathbf{R}(\boldsymbol{\tau})$ is the correlation matrix given by (20). The vector $\boldsymbol{\chi}(\tilde{u}, \boldsymbol{\tau})$ is given by

$$\boldsymbol{\chi}(\tilde{u}, \boldsymbol{\tau}) = \int_0^T r(\tilde{u}, t) \begin{bmatrix} w(t - \tau_1) \\ w(t - \tau_2) \\ \vdots \\ w(t - \tau_L) \end{bmatrix} dt \quad (14)$$

where the entries of $\boldsymbol{\chi}(\tilde{u}, \boldsymbol{\tau})$ can be interpreted as the correlation of the received signal $r(\tilde{u}, t)$ with $w(t)$ at different hypothesized delays.

For a wide bandwidth transmission channel, it is often assumed that the propagation channel is separable, i.e.,

$$|\tau_i - \tau_j| > D \quad \text{for all} \quad i \neq j \quad (15)$$

where $D \triangleq$ the width of $w(t)$. Under the assumption of a separable multipath channel, the ML estimates of $\hat{\boldsymbol{\tau}}(\tilde{u})$ and $\hat{\mathbf{c}}(\tilde{u})$ based on $r(\tilde{u}, t)$ are derived in Appendix B as

$$\hat{\boldsymbol{\tau}}(\tilde{u}) = \underset{\boldsymbol{\tau}: |\tau_i - \tau_j| > D}{\operatorname{argmax}} \left\{ \sum_{i=1}^L \left| \frac{\chi(\tilde{u}, \tau_i)}{\sqrt{R(0)}} \right| \right\} \quad (16)$$

and

$$\hat{\mathbf{c}}(\tilde{u}) = \frac{\boldsymbol{\chi}(\tilde{u}, \hat{\boldsymbol{\tau}}(\tilde{u}))}{R(0)} \quad (17)$$

where $R(0) = \int_0^T |w(t)|^2 dt$, and the elements of $\boldsymbol{\tau}$ satisfy the condition given in (15). The $\chi(\tilde{u}, \tau_i)$ is the i^{th} component of the vector $\boldsymbol{\chi}(\tilde{u}, \boldsymbol{\tau})$ given by (14). Note that the ML estimates of $\hat{\boldsymbol{\tau}}(\tilde{u})$

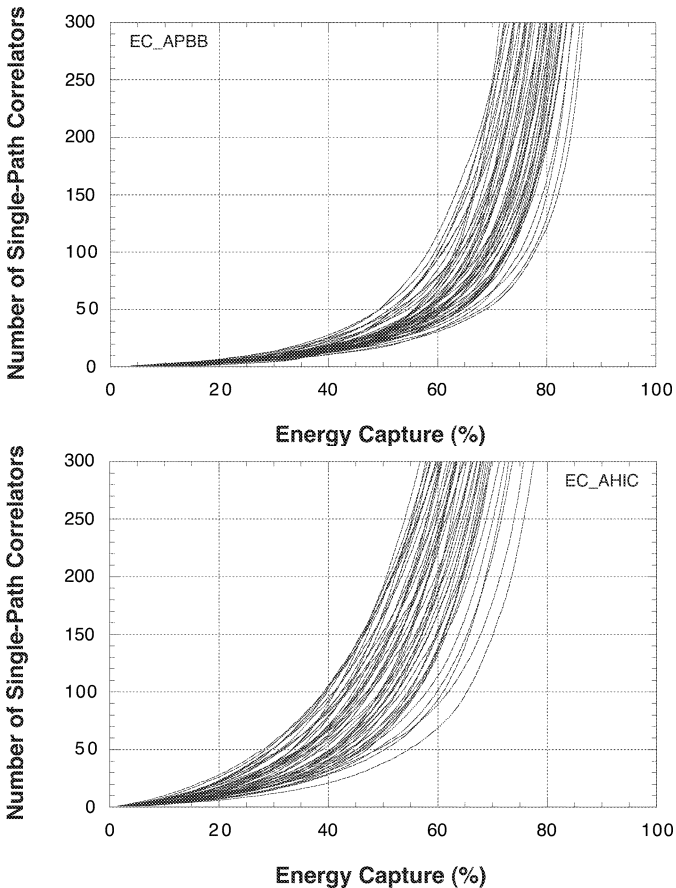


Fig. 10. The number of single-path signal correlators in a UWB Rake receiver as a function of percentage energy capture for received waveforms in an office P (upper plot) and H (lower plot) representing typical “high SNR” and “low SNR” environment. In each plot, 49 measurement waveforms are used.

and $\hat{c}(\tilde{u})$ result in decoupled solutions under the assumption of a separable multipath channel.

3) *Performance Measure and Results of the ML Multipath Detector*: The performance of the multipath detector can be measured in terms of the quantity *energy capture*. Energy capture as a function of L for each observation $r(\tilde{u}, t)$ is defined mathematically as

$$EC(\tilde{u}, L) \triangleq 1 - \underbrace{\frac{\mathcal{E}_{\min}(\tilde{u}, L)}{E_{\text{tot}}(\tilde{u})}}_{\triangleq \text{normalized MSE}} \quad (18)$$

where $E_{\text{tot}}(\tilde{u})$ is the total energy in the received waveform $r(\tilde{u}, t)$ given by (4). Equation (18) can be interpreted as the fraction of the received waveform energy captured by the UWB SRake receiver consisting of L single-path signal correlators.

Energy capture as a function of the number of single-path signal correlators is computed for each received waveform measurement. This can be used to estimate the performance of a selective Rake receiver with coherent diversity combining of L correlator outputs, each correlator matched to a basic building block waveform $w(t)$. The number of required correlators in a UWB SRake receiver versus percentage energy capture is plotted in Fig. 10, based on the ML estimators given in (16) and (17), for each of the measured channels in offices

P and H representing a typical “high SNR” and “low SNR” environment.⁸ In generating this figure, we have used $w(t)$ as the average LOS component extracted from the “clean” pulse measurements in Fig. 3. Recall from Section II-C that the first 10 ns of the recorded waveforms in Fig. 3 represent a clean pulse arriving via the direct LOS path and are not corrupted by multipath components.

Note in Fig. 10 that the amount of captured energy increases rapidly as the number of correlators increases from 0 to 50. However, this improvement becomes gradual as the number of correlators increases from 50 to 100. Beyond this point, only a negligible improvement in energy capture can be made. Because of complexity constraints in practice, UWB SRake receivers are designed to operate in the regions where the increase in energy capture as a function of the number of correlators is rapid. Fig. 10 also suggests that the number of dominant specular multipath components is expected to be less than 50 for UWB signal transmissions in a typical modern office building. On the other hand, the number of dominant specular multipath components is much larger than five.

While the multipath model which motivates the model-based characterization in Section III-B may be questioned, the signal strengths identified by correlation with $w(t)$ are based on actual measurements. These can be used to predict the performance of a simple binary PPM with the same transmitted pulse shape, running over the same measured channel, and using a correlation receiver with the template waveform $\hat{s}(\tilde{u}, t)$. The curves in Fig. 11 indicate the projected BEP performance of such UWB SRake receiver as a function of SNR and the number of single-path signal correlators implemented (i.e., “paths” tracked). It is assumed that the receiver chooses the delays and amplitudes to optimize performance using (16) and (17). That is, the UWB PPM SRake receiver with the pictured performance implements a maximum-energy-capture algorithm for a given number L of correlators. Notice that there is a somewhat wider spread between the $L = 1$ and $L = 128$ in the low SNR case in Fig. 11, indicating that there is slightly more to be gained for large L . The SNR offset between a curve in the low SNR environment and the corresponding curve in the high SNR environment can be determined roughly from the data of Table I or Fig. 7.

IV. CONCLUSION

The signal propagation experiment described here was performed in a typical modern laboratory/office building to characterize indoor UWB signal propagation channels. The bandwidth of the signal used in this experiment was in excess of 1 GHz, resulting in a differential path delay resolution of less than a nanosecond without special processing. Robustness of the UWB signal to fades is quantified through histograms and cumulative distributions of the signal quality in various locations of the building. The results demonstrate that a UWB signal in this environment does not suffer deep fades and that UWB radios

⁸The “usual” separable channel assumptions given in (15) may not always be valid, even in the case of UWB transmissions channels. However, the ML estimators derived under this assumption are used in computations for simplicity. The optimal solution in the case of nonseparable multipath is computation intensive. One suboptimal approach in this case is to use the CLEAN algorithm, and an example of its application to UWB propagation channels can be found in [36].

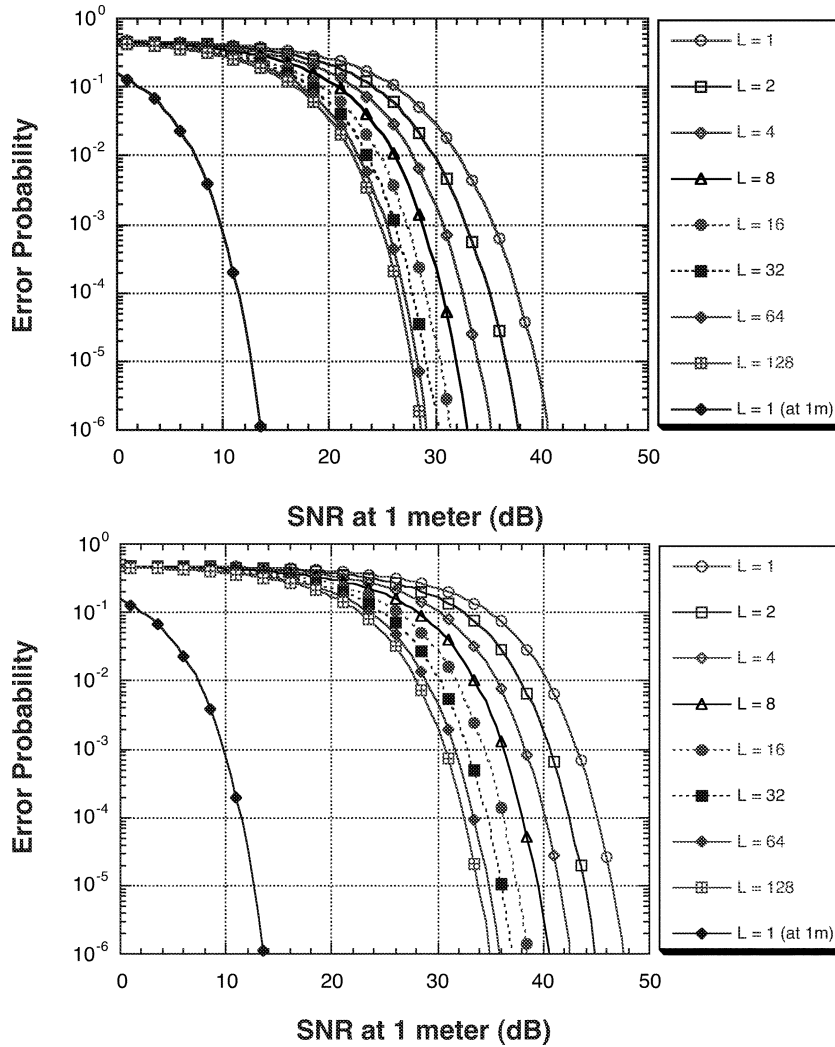


Fig. 11. BEP performance of selective Rake receiver in an office P (upper plot) and H (lower plot) representing typical “high SNR” and “low SNR” environment. In each plot, 49 measurement waveforms are used.

have the potential for robust indoor operation at low transmitted power levels.

ARake receivers and SRake receivers have been discussed. The ARake receiver serves as the best case (bench mark) for a Rake receiver design and lower bounds the performance degradation caused by multipath. Typical ensembles of ARake auto-correlation functions suggest that multipath places some limit on the ability to extend PPM techniques to the M -ary case. These results must be taken into account when designing data modulation schemes that provide robust, simple, high-rate communication capability in the presence of multipath.

Multipath components of measured waveforms are determined using a ML estimator which is based on a separable specular multipath channel model. Energy capture (and, consequently, BEP for an SRake receiver using a maximum-energy-capture policy) as a function of the number of single-path signal correlators used in an UWB SRake receiver shows that the number of dominant specular multipath components is typically less than 50 for UWB signal transmissions in a typical modern laboratory/office building. On the other hand, the number of dominant specular multipath components is much

larger than five, which suggests that ray tracing techniques may not be feasible for these UWB indoor wireless communications channels.

The results for model-based characterization presented in Section III-B are based on the simple template structure suggested by the specular model given in (2). However, more complicated template structures are possible at the expense of receiver complexity. One such example is the use of a family of basic building block waveforms $\{w^l(t)\}_{l=1}^N$ and determination of the “best” choice of $\{\{\hat{c}_i^l(\tilde{u})\}_{i=1}^L, \{\hat{\tau}_i^l(\tilde{u})\}_{i=1}^L\}_{l=1}^N$ such that the synthesized waveform $\sum_{l=1}^N \sum_{i=1}^L \hat{c}_i^l(\tilde{u}) w^l(t - \hat{\tau}_i^l(\tilde{u}))$ is well matched to the received waveform $s(\tilde{u}, t)$.

APPENDIX ML MULTIPATH DETECTOR

It can be shown that the ML estimates of the amplitude vector $\hat{\mathbf{c}}(\tilde{u})$ and delay vector $\hat{\boldsymbol{\tau}}(\tilde{u})$ are the values \mathbf{c} and $\boldsymbol{\tau}$ that *minimize* the statistic

$$S(\mathbf{c}, \boldsymbol{\tau}) = \mathbf{c}^\dagger \mathbf{R}(\boldsymbol{\tau}) \mathbf{c} - \mathbf{c}^\dagger \boldsymbol{\chi}(\tilde{u}, \boldsymbol{\tau}) - \boldsymbol{\chi}^\dagger(\tilde{u}, \boldsymbol{\tau}) \mathbf{c}. \quad (19)$$

The correlation matrix $\mathbf{R}(\boldsymbol{\tau})$ is a function of $\boldsymbol{\tau}$ and is given by

$$\mathbf{R}(\boldsymbol{\tau}) = \begin{bmatrix} R(\tau_1 - \tau_1) & R(\tau_1 - \tau_2) & \cdots & R(\tau_1 - \tau_L) \\ R(\tau_2 - \tau_1) & R(\tau_2 - \tau_2) & \cdots & R(\tau_2 - \tau_L) \\ \vdots & \vdots & \ddots & \vdots \\ R(\tau_L - \tau_1) & R(\tau_L - \tau_2) & \cdots & R(\tau_L - \tau_L) \end{bmatrix} \quad (20)$$

with each entry of the matrix is

$$R(\tau_i - \tau_j) = \int_0^T w(t - \tau_i) w(t - \tau_j) dt. \quad (21)$$

The vector $\boldsymbol{\chi}(\tilde{u}, \boldsymbol{\tau})$ is given by

$$\boldsymbol{\chi}(\tilde{u}, \boldsymbol{\tau}) = \int_0^T r(\tilde{u}, t) \begin{bmatrix} w(t - \tau_1) \\ w(t - \tau_2) \\ \vdots \\ w(t - \tau_L) \end{bmatrix} dt \quad (22)$$

where the components of $\boldsymbol{\chi}(\tilde{u}, \boldsymbol{\tau})$ can be interpreted as the correlation of the received signal $r(\tilde{u}, t)$ with $w(t)$ at different hypothesized delays. Let

$$\boldsymbol{\lambda}(\tilde{u}, \boldsymbol{\tau}) = \mathbf{R}^{-1}(\boldsymbol{\tau}) \boldsymbol{\chi}(\tilde{u}, \boldsymbol{\tau}). \quad (23)$$

Then, adding and subtracting the quantity $\boldsymbol{\lambda}^\dagger(\tilde{u}, \boldsymbol{\tau}) \mathbf{R}(\boldsymbol{\tau}) \boldsymbol{\lambda}(\tilde{u}, \boldsymbol{\tau})$, and regrouping like terms, gives

$$S(\mathbf{c}, \boldsymbol{\tau}) = \underbrace{[\mathbf{c} - \boldsymbol{\lambda}(\tilde{u}, \boldsymbol{\tau})]^\dagger \mathbf{R}(\boldsymbol{\tau}) [\mathbf{c} - \boldsymbol{\lambda}(\tilde{u}, \boldsymbol{\tau})]}_{\triangleq A} - \underbrace{\boldsymbol{\lambda}^\dagger(\tilde{u}, \boldsymbol{\tau}) \mathbf{R}(\boldsymbol{\tau}) \boldsymbol{\lambda}(\tilde{u}, \boldsymbol{\tau})}_{\triangleq B}. \quad (24)$$

Note that A and B are nonnegative quadratic forms with B independent of the choice of \mathbf{c} , so that $S(\mathbf{c}, \boldsymbol{\tau})$ is minimized when $A = 0$ by choice of \mathbf{c} , and

$$B = \boldsymbol{\lambda}^\dagger(\tilde{u}, \boldsymbol{\tau}) \mathbf{R}(\boldsymbol{\tau}) \boldsymbol{\lambda}(\tilde{u}, \boldsymbol{\tau}) = \boldsymbol{\chi}^\dagger(\tilde{u}, \boldsymbol{\tau}) \mathbf{R}^{-1}(\boldsymbol{\tau}) \boldsymbol{\chi}(\tilde{u}, \boldsymbol{\tau}) \quad (25)$$

is maximized over $\boldsymbol{\tau}$. The condition $A = 0$ implies that

$$\mathbf{c} = \boldsymbol{\lambda}(\tilde{u}, \boldsymbol{\tau}) = \mathbf{R}^{-1}(\boldsymbol{\tau}) \boldsymbol{\chi}(\tilde{u}, \boldsymbol{\tau}). \quad (26)$$

Therefore, ML estimates of the delay vector $\hat{\boldsymbol{\tau}}$ and amplitude vector $\hat{\mathbf{c}}$ are

$$\hat{\boldsymbol{\tau}}(\tilde{u}) = \underset{\boldsymbol{\tau}}{\operatorname{argmax}} \left\{ \boldsymbol{\chi}^\dagger(\tilde{u}, \boldsymbol{\tau}) \mathbf{R}^{-1}(\boldsymbol{\tau}) \boldsymbol{\chi}(\tilde{u}, \boldsymbol{\tau}) \right\} \quad (27)$$

and

$$\hat{\mathbf{c}}(\tilde{u}) = \mathbf{R}^{-1}(\hat{\boldsymbol{\tau}}(\tilde{u})) \boldsymbol{\chi}(\tilde{u}, \hat{\boldsymbol{\tau}}(\tilde{u})). \quad (28)$$

APPENDIX

ML MULTIPATH DETECTOR FOR A SEPARABLE CHANNEL

When the propagation channel is separable, then $R(\tau_i - \tau_j) = 0$ for all $i \neq j$ and the correlation matrix $\mathbf{R}(\boldsymbol{\tau})$ becomes

$$\mathbf{R} = \begin{bmatrix} R(0) & 0 & \cdots & 0 \\ 0 & R(0) & \cdots & 0 \\ \vdots & \vdots & \ddots & \vdots \\ 0 & 0 & \cdots & R(0) \end{bmatrix}$$

where $R(0) = \int_0^T |w(t)|^2 dt$. Note that $\mathbf{R}(\boldsymbol{\tau})$ is independent of $\boldsymbol{\tau}$ in this case and simple matrix manipulation shows that

$$\boldsymbol{\chi}^\dagger(\tilde{u}, \boldsymbol{\tau}) \mathbf{R}^{-1} \boldsymbol{\chi}(\tilde{u}, \boldsymbol{\tau}) = \sum_{i=1}^L \frac{1}{R(0)} |\chi(\tilde{u}, \tau_i)|^2 \quad (29)$$

where

$$\chi(\tilde{u}, \tau_i) = \int_0^T r(\tilde{u}, t) w(t - \tau_i) dt. \quad (30)$$

Therefore, the ML estimates of $\hat{\boldsymbol{\tau}}(\tilde{u})$ and $\hat{\mathbf{c}}(\tilde{u})$ based on a specific observation $r(\tilde{u}, t)$ become

$$\hat{\boldsymbol{\tau}}(\tilde{u}) = \underset{\boldsymbol{\tau}: |\tau_i - \tau_j| > D}{\operatorname{argmax}} \left\{ \sum_{i=1}^L \left| \frac{\chi(\tilde{u}, \tau_i)}{\sqrt{R(0)}} \right| \right\} \quad (31)$$

and

$$\hat{\mathbf{c}}(\tilde{u}) = \frac{\boldsymbol{\chi}(\tilde{u}, \hat{\boldsymbol{\tau}}(\tilde{u}))}{R(0)}. \quad (32)$$

ACKNOWLEDGMENT

The authors wish to thank the Time Domain Corporation for its assistance and support for the propagation measurement experiments described herein.

REFERENCES

- [1] G. F. Ross, "The transient analysis of certain TEM mode four-post networks," *IEEE Trans. Microwave Theory Technol.*, vol. 14, p. 528, Nov. 1966.
- [2] C. L. Bennett and G. F. Ross, "Time-domain electromagnetics and its applications," *Proc. IEEE*, vol. 66, pp. 299–318, Mar. 1978.
- [3] M. Z. Win and R. A. Scholtz, "Impulse radio: How it works," *IEEE Commun. Lett.*, vol. 2, pp. 36–38, Feb. 1998.
- [4] —, "Comparisons of analog and digital impulse radio for multiple-access communications," in *Proc. IEEE Int. Conf. Communication*, vol. 1, June 1997, pp. 91–95.
- [5] M. Z. Win, X. Qiu, R. A. Scholtz, and V. O. K. Li, "ATM-based TH-SSMA network for multimedia PCS," *IEEE J. Select. Areas Commun.*, vol. 17, pp. 824–836, May 1999.
- [6] M. Z. Win and R. A. Scholtz, "Ultra-wide bandwidth time-hopping spread-spectrum impulse radio for wireless multiple-access communications," *IEEE Trans. Commun.*, vol. 48, pp. 679–691, Apr. 2000.
- [7] M. Z. Win, "A unified spectral analysis of generalized time-hopping spread-spectrum signals in the presence of timing jitter," *IEEE J. Select. Areas Commun.*, vol. 20, pp. XXX–XXX, Dec. 2002, to be published.
- [8] S. S. Kolenchery, J. K. Townsend, J. A. Freebersyser, and G. Billbro, "Performance of local power control in peer-to-peer impulse radio networks with bursty traffic," in *Proc. IEEE Global Telecommunications Conf.*, vol. 2, Nov. 1997, pp. 910–916.
- [9] S. S. Kolenchery, J. K. Townsend, and J. A. Freebersyser, "A novel impulse radio network for tactical military wireless communications," in *Proc. Military Communications Conf.*, vol. 1, Boston, MA, Oct. 1998, pp. 59–65.
- [10] G. D. Weeks, J. K. Townsend, and J. A. Freebersyser, "Performance of hard decision detection for impulse radio," in *Proc. Military Communications Conf.*, vol. 2, Atlantic City, NJ, Oct. 1999, pp. 1201–1206.
- [11] J. Conroy, J. L. LoCicero, and D. R. Ucci, "Communication techniques using monopulse waveforms," in *Proc. Military Communications Conf.*, vol. 2, Atlantic City, NJ, Oct. 1999, pp. 1181–1185.
- [12] H. Lee, B. Han, Y. Shin, and S. Im, "Multipath characteristics of impulse radio channels," in *Proc. 50th Annu. Int. Vehicle Technology Conf.*, vol. 3, Tokyo, Japan, 2000, pp. 2487–2491.
- [13] C. J. Le Martret and G. B. Giannakis, "All-digital PAM impulse radio for multiple-access through frequency-selective multipath," in *Proc. IEEE Global Telecommunications Conf.*, vol. 1, Nov. 2000, pp. 77–81.
- [14] L. Zhao and A. M. Haimovich, "Interference suppression in ultra-wide-band communications," in *Proc. Conf. Information Science, System*, vol. 2, Baltimore, MD, Mar. 2001, pp. 759–763.

- [15] L. Zhao, A. M. Haimovich, and H. Grebel, "Performance of ultra-wide-band communications in the presence of interference," in *Proc. IEEE Int. Conf. Communications*, vol. 10, June 2001, pp. 2948–2952.
- [16] L. Zhao, A. M. Haimovich, and M. Z. Win, "Capacity of ultra-wide bandwidth communications over multipath channels," in *Proc. IEEE Int. Symp. Advances Wireless Communications*, Victoria, Canada, Sept. 2002.
- [17] M. Z. Win, R. A. Scholtz, and M. A. Barnes, "Ultra-wide bandwidth signal propagation for indoor wireless communications," in *Proc. IEEE Int. Conf. Communications*, vol. 1, June 1997, pp. 56–60.
- [18] M. Z. Win and R. A. Scholtz, "On the robustness of ultra-wide bandwidth signals in dense multipath environments," *IEEE Commun. Lett.*, vol. 2, pp. 51–53, Feb. 1998.
- [19] —, "On the energy capture of ultra-wide bandwidth signals in dense multipath environments," *IEEE Commun. Lett.*, vol. 2, pp. 245–247, Sept. 1998.
- [20] P. A. Bello, "Characterization of randomly time-variant linear channels," *IEEE Trans. Commun. Syst.*, vol. COM-11, pp. 360–393, Dec. 1963.
- [21] W. C. Jakes, Ed., *Microwave Mobile Communications*. Piscataway, NJ: IEEE Press, 1995.
- [22] R. Steele and L. Hanzo, *Mobile Radio Communications: Second and Third Generation Cellular and WATM Systems*, 2nd ed. New York: Wiley, 1999.
- [23] K. Pahlavan and A. H. Levesque, *Wireless Information Networks*, 1st ed. New York: Wiley, 1995.
- [24] T. S. Rappaport, *Wireless Communications*, 1st ed. Upper Saddle River, NJ: Prentice-Hall, 1996.
- [25] R. S. Kennedy, *Fading Dispersive Communication Channels*, 1st ed. New York: Wiley, 1969.
- [26] J. D. Parsons, *The Mobile Radio Propagation Channel*, 1st ed. New York: Wiley, 1992.
- [27] J. B. Andersen, T. S. Rappaport, and S. Yoshida, "Propagation measurements and models for wireless communications channels," *IEEE Commun. Mag.*, vol. 33, pp. 42–49, Jan. 1995.
- [28] T. S. Rappaport, S. Y. Seidel, and K. Takamizawa, "Statistical channel impulse response models for factory an open plan building radio communication system design," *IEEE Trans. Commun.*, vol. 39, pp. 794–807, May 1991.
- [29] S. Y. Seidel and T. S. Rappaport, "914 MHz path loss prediction models for indoor wireless communications in multifloored buildings," *IEEE Trans. Antennas Propagat.*, vol. 40, pp. 207–217, Feb. 1992.
- [30] D. M. J. Devasirvatham, "Multipath time delay jitter measured at 850 MHz in the portable radio environment," *IEEE J. Select. Areas Commun.*, vol. SAC-5, pp. 855–861, June 1987.
- [31] A. A. Saleh and R. A. Valenzuela, "A statistical model for indoor multipath propagation," *IEEE J. Select. Areas Commun.*, vol. SAC-5, pp. 128–137, Feb. 1987.
- [32] R. A. Valenzuela, O. Landron, and D. L. Jacobs, "Estimating local mean signal strength of indoor multipath propagation," *IEEE Trans. Veh. Technol.*, vol. 46, pp. 203–212, Feb. 1997.
- [33] R. J. Bultitude, S. A. Mahmoud, and W. A. Sullivan, "A comparison of indoor radio propagation characteristics at 910 MHz and 1.75 GHz," *IEEE J. Select. Areas Commun.*, vol. 7, pp. 20–30, Jan. 1989.
- [34] H. Hashemi, "The indoor radio propagation channel," *Proc. IEEE*, vol. 81, pp. 943–968, July 1993.
- [35] Q. Spencer, B. Jeffs, M. Jensen, and A. Swindlehurst, "Modeling the statistical time and angle of arrival characteristics of an indoor multipath channel," *IEEE J. Select. Areas Commun.*, vol. 18, pp. 347–360, Mar. 2000.
- [36] R. J.-M. Cramer, R. A. Scholtz, and M. Z. Win, "An evaluation of the ultra-wideband propagation channel," *IEEE Trans. Antennas Propagat.*, vol. 50, pp. 561–570, May 2002.
- [37] G. Turin, F. D. Clapp, T. L. Johnston, S. B. Fine, and D. Lavry, "A statistical model of urban multipath propagation," *IEEE Trans. Veh. Technol.*, vol. VT-21, pp. 1–9, Feb. 1972.
- [38] G. Turin, "Introduction to spread-spectrum antimultipath techniques and their application to urban digital radio," *Proc. IEEE*, vol. 68, pp. 328–353, Mar. 1980.
- [39] H. Suzuki, "A statistical model for urban radio propagation," *IEEE Trans. Commun.*, vol. 25, pp. 673–680, July 1977.
- [40] H. Hashemi, "Simulation of the urban radio propagation channel," *IEEE Trans. Veh. Technol.*, vol. VT-28, pp. 213–225, Aug. 1979.
- [41] D. C. Cox, "Delay Doppler characteristics of multipath propagation at 910 MHz in a suburban mobile radio environment," *IEEE Trans. Antennas Propagat.*, vol. AP-20, pp. 625–635, Sept. 1972.
- [42] —, "Time- and frequency-domain characterizations of multipath propagation at 910 MHz in a suburban mobile-radio environment," *Radio Sci.*, pp. 1069–1077, Dec. 1972.
- [43] —, "910 MHz urban mobile radio propagation: Multipath characteristics in New York city," *IEEE Trans. Commun.*, vol. COM-21, pp. 1188–1194, Nov. 1973.
- [44] D. C. Cox and R. P. Leck, "Distributions of multipath delay spread and average excess delay for 910-MHz urban mobile radio paths," *IEEE Trans. Antennas Propagat.*, vol. AP-23, pp. 206–213, Mar. 1975.
- [45] D. L. Nielson, "Microwave propagation measurements for mobile digital radio application," *IEEE Trans. Veh. Technol.*, vol. VT-28, pp. 117–132, Aug. 1978.
- [46] V. Erceg, A. J. Rustako Jr, and R. S. Roman, "Diffraction around corners and its effects on the microcell coverage area in urban and suburban environments at 900 MHz, 2 GHz, and 6 GHz," *IEEE Trans. Veh. Technol.*, vol. 43, pp. 762–766, Aug. 1994.
- [47] E. S. Sousa, V. M. Jovanović, and C. Daigneault, "Delay spread measurements for the digital cellular channel in Toronto," *IEEE Trans. Veh. Technol.*, vol. 43, pp. 837–847, Nov. 1994.
- [48] L. J. Greenstein, V. Erceg, Y. S. Yeh, and M. V. Clark, "A new path-gain/delay-spread propagation model for digital cellular channels," *IEEE Trans. Veh. Technol.*, vol. 46, pp. 477–485, May 1997.
- [49] D. Cassioli, M. Z. Win, and A. F. Molisch, "The ultra-wide bandwidth indoor channel: From statistical model to simulations," *IEEE J. Select. Areas Commun.*, vol. 20, pp. 1247–1257, Aug. 2002.
- [50] E. T. Whittaker, "On the functions which are represented by the expansions of the interpolation theory," in *Proc. Roy. Soc. Edinburgh*, vol. 35, 1915, pp. 181–194.
- [51] J. M. Whittaker, "The Fourier theory of the cardinal functions," in *Proc. Math. Soc. Edinburgh*, vol. 1, 1929, pp. 169–176.
- [52] R. V. L. Hartley, "The transmission of information," *Bell Syst. Tech. J.*, vol. 7, pp. 535–560, 1928.
- [53] H. Nyquist, "Certain topics in telegraph transmission theory," *AIEE Trans.*, vol. 47, pp. 617–644, Apr. 1928.
- [54] C. E. Shannon, "Communications in the presence of noise," *Proc. IRE*, vol. 37, pp. 10–21, Jan. 1949.
- [55] D. Slepian, "On bandwidth," *Proc. IEEE*, vol. 64, pp. 292–300, Mar. 1976.
- [56] A. J. Jerri, "The Shannon sampling theorem – Its various extensions and applications: A tutorial review," *Proc. IEEE*, vol. 65, pp. 1565–1596, Nov. 1977.
- [57] H. G. Schantz and L. Fullerton, "The diamond dipole: A Gaussian impulse antenna," in *Proc. IEEE AP-S Int. Symp. USNC/URSI National Radio Science Meeting*, vol. 4, July 2001, pp. 100–103.
- [58] "Revision of Part 15 of the Commission's Rules Regarding Ultra-Wideband Transmission Systems," Federal Communications Commission, ET Docket 98–153, 2002.
- [59] R. Durrett, *Probability: Theory and Examples*, first ed. Pacific Grove, CA: Wadsworth, 1991.
- [60] M. K. Simon, S. M. Hinedi, and W. C. Lindsey, *Digital Communication Techniques: Signal Design and Detection*, 1st ed. Englewood Cliffs, NJ: Prentice-Hall, 1995.
- [61] R. C. Robertson and M. A. Morgan, "Ultra-wideband impulse receiving antenna design and evaluation," in *Ultra-Wideband Short Pulse Electromagnetics 2*, L. Carin and L. B. Felsen, Eds. New York: Plenum, 1995, pp. 179–196.
- [62] J. G. Maloney, G. S. Smith, and W. R. Scott Jr, "Accurate computation of the radiation from simple antennas using the finite-difference time-domain method," *IEEE Trans. Antennas Propagat.*, vol. 38, pp. 1059–1068, July 2000.
- [63] R. Price and P. E. Green Jr, "A communication technique for multipath channels," *Proc. IRE*, vol. 46, pp. 555–570, Mar. 1958.
- [64] J. G. Proakis, *Digital Communications*, 4th ed. New York: McGraw-Hill, 2001.
- [65] P. J. Bickel and K. Doksum, *Mathematical Statistics: Basic Ideas and Selected Topics*, 1st ed. Oakland, CA: Holden-Day, 1977.
- [66] M. Z. Win and Z. A. Kostić, "Virtual path analysis of selective Rake receiver in dense multipath channels," *IEEE Commun. Lett.*, vol. 3, pp. 308–310, Nov. 1999.
- [67] M. Z. Win, G. Chrisikos, and N. R. Sollenberger, "Effects of chip rate on selective Rake combining," *IEEE Commun. Lett.*, vol. 4, pp. 233–235, July 2000.
- [68] M. Z. Win and Z. A. Kostić, "Impact of spreading bandwidth on Rake reception in dense multipath channels," *IEEE J. Select. Areas Commun.*, vol. 17, pp. 1794–1806, Oct. 1999.
- [69] M. Z. Win, G. Chrisikos, and N. R. Sollenberger, "Performance of Rake reception in dense multipath channels: Implications of spreading bandwidth and selection diversity order," *IEEE J. Select. Areas Commun.*, vol. 18, pp. 1516–1525, Aug. 2000.
- [70] M. Z. Win and G. Chrisikos, "Impact of spreading bandwidth and selection diversity order on selective Rake reception," in *Wideband Wireless Digital Communications*, A. F. Molisch, Ed. Upper Saddle River, NJ: Prentice-Hall, 2001, pp. 424–454.

- [71] M. Z. Win, G. Chrisikos, A. F. Molisch, and N. R. Sollenberger, "Selective Rake diversity in multipath fading with arbitrary power delay profile," in *Proc. IEEE Global Telecommunications Conf.*, vol. 2, Dec. 2000, pp. 960–964.
- [72] D. Cassioli, M. Z. Win, F. Vatalaro, and A. F. Molisch, "Performance of selective Rake reception in a realistic UWB channel," in *Proc. IEEE Int. Conf. Communications*, vol. 2, May 2002, pp. 763–767.
- [73] C. L. Weber, *Elements of Detection and Signal Design*, 1st ed. New York: Springer-Verlag, 1987.
- [74] F. Ramírez-Mireles, M. Z. Win, and R. A. Scholtz, "Signal selection for the indoor wireless impulse radio channel," in *Proc. 47th Annu. Int. Vehicular Technology Conf.*, Phoenix, AZ, May 1997, pp. 2243–2247.



Moe Z. Win (S'85–M'87–SM'97) received the B.S. degree (*magna cum laude*) from Texas A&M University, College Station, and the M.S. degree from the University of Southern California (USC), Los Angeles, in 1987 and 1989, respectively, in electrical engineering. As a Presidential Fellow at USC, he received both an M.S. degree in applied mathematics and the Ph.D. degree in electrical engineering in 1998. He is a Distinguished Alumnus of Mountain View College.

In 1987, he joined the Jet Propulsion Laboratory (JPL), California Institute of Technology, Pasadena, where he performed research on digital communications and optical systems for NASA space exploration missions. From 1994 to 1997, he was a Research Assistant with the Communication Sciences Institute at USC, where he played a key role in the successful creation of the Ultra-Wideband Radio Laboratory. From 1998 to 2002, he was with the Wireless Systems Research Department, AT&T Laboratories-Research, Middletown, NJ. During that time, he performed research on several aspects of high-data-rate multiple-access systems and made fundamental contributions to communication theory and its application to wideband wireless transmission. In 2000, he was promoted to a Principal Technical Staff Member. Since 2002, he has been with the Laboratory for Information and Decision Systems (LIDS), Massachusetts Institute of Technology, Cambridge, where he holds the Charles Stark Draper Chair. His main research interests are the application of communication, detection, and estimation theories to a variety of communications problems including time-varying channels, diversity, equalization, synchronization, signal design, ultrawide-bandwidth communication, and optical communications.

Dr. Win has been involved actively in organizing and chairing sessions and has served as a Member of the Technical Program Committee in a number of international conferences. He currently serves as the Technical Program Chair for the IEEE Communication Theory Symposium of ICC-2004. He served as the Technical Program Chair for the IEEE Communication Theory Symposium of Globecom-2000 and the IEEE Conference on Ultra-Wideband Systems and Technologies (2002), Technical Program Vice-Chair for the IEEE International Conference on Communications (2002), and the Tutorial Chair for the IEEE Semiannual International Vehicular Technology Conference (Fall-2001). He is the secretary for the Radio Communications Technical Committee, the current Editor for *Equalization and Diversity* for the IEEE TRANSACTIONS ON COMMUNICATIONS and a Guest Editor for the 2002 IEEE JOURNAL ON SELECTED AREAS IN COMMUNICATIONS, Special Issue on Ultra-Wideband Radio in Multiaccess Wireless Communications. He is a member of Eta Kappa Nu, Tau Beta Pi, Pi Mu Epsilon, Phi Theta Kappa, and Phi Kappa Phi. He was a University Undergraduate Fellow at Texas A&M University, where he received, among others awards, the Academic Excellence Award. At USC, he received several awards including the Outstanding Research Paper Award and the Phi Kappa Phi Student Recognition Award. He was the recipient of the IEEE Communications Society Best Student Paper Award at the Fourth Annual IEEE NetWorld+Interop '97 Conference.



Robert A. Scholtz (S'56–M'59–SM'73–F'80–LF'02) was born in Lebanon, OH, on January 26, 1936. He is a Distinguished Alumnus of the University of Cincinnati, where, as a Sheffield Scholar, he received the E.E. degree in 1958. He was a Hughes Masters and Doctoral Fellow while obtaining the M.S. and Ph.D. degrees in electrical engineering from University of Southern California (USC), Los Angeles, in 1960, and Stanford University in 1964, respectively.

While working on missile radar signal processing problems, he remained part-time at Hughes Aircraft Company until 1978. In 1963, he joined the faculty of the University of Southern California, where he is now Professor of Electrical Engineering. From 1984 to 1989, he served as Director of USC's Communication Sciences Institute. He was Chairman of the Electrical Engineering Systems Department from 1994 to 2000. In 1996, as part of the Integrated Media Systems Center effort, he was instrumental in forming the Ultra-wideband Radio Laboratory (UltRa Lab) to provide facilities for the design and test of impulse radio systems and other novel high-bandwidth high-data-rate wireless mobile communication links. He has consulted for the LinCom Corporation, Axiomatix, Inc., the Jet Propulsion Laboratory, Technology Group, TRW, Pulson Communications (Time Domain Corporation), and Qualcomm, as well as various government agencies. His research interests include communication theory, synchronization, signal design, coding, adaptive processing, and pseudonoise generation, and their application to communications and radar systems. He has co-authored *Spread Spectrum Communications* with M. K. Simon, J. K. Omura, and B. K. Levitt, and *Basic Concepts in Information Theory and Coding* with S. W. Golomb and R. E. Peile. He has been General Chairman of five workshops in the area of communications, including most recently the Ultrawideband Radio Workshop held in May 1998, and has been an active participant on NSF panels and in research planning workshops of the U.S. Army Research Office.

Dr. Scholtz was elected to the grade of Fellow in the IEEE, "for contributions to the theory and design of synchronizable codes for communications and radar systems" in 1980. In 1983, he received the Leonard G. Abraham Prize Paper Award for the historical article, "The Origins of Spread Spectrum Communications;" this same paper received the 1984 Donald G. Fink Prize Award given by the IEEE. His paper "Acquisition of Spread-Spectrum Signals by an Adaptive Array" with D. M. Dlugos received the 1992 Senior Award of the IEEE Signal Processing Society. His paper "Strategies for minimizing the intercept time in a mobile communication network with directive/adaptive antennas," with J.-H. Oh received the Ellersick Award for the best unclassified paper at Milcom 1997. His paper "ATM Based Ultrawide Bandwidth (UWB) Multiple-Access Radio Network for Multimedia PCS" with students M. Z. Win, J. H. Ju, X. Qiu, and colleague V. O. K. Li received the best student paper award from the NetWorld+Interop'97 program committee. In 2001, he received the Military Communications Conference Award for Technical Achievement. He has been an active member of the IEEE for many years, manning important organizational posts, including Finance Chairman for the 1977 National Telecommunications Conference, Program Chairman for the 1981 International Symposium on Information Theory, and IEEE Board of Governors positions for the IEEE Information Theory Group and the Communications Society.